PCCP

Accepted Manuscript

ROYAL SOCIETY OF CHEMISTRY

www.rsc.org/pccp

Cite this: DOI: 10.1039/c0xx00000x

www.rsc.org/xxxxxx

ARTICLE TYPE

DFT Study on the Interaction between Glycine Molecules/Radicals with (8, 0) SiCNT

Kefu Gao,[a] Guanghui Chen,*[a] and Di Wu[b]

Received (in XXX, XXX) Xth XXXXXXXXX 20XX, Accepted Xth XXXXXXXXX 20XX

DOI: 10.1039/b000000x

The geometrical structures, energetics and electronic properties of glycine molecules as well as dehydrogenated radicals interaction with silicon carbide nanotubes (SiCNTs) are investigated based on density functional theory (DFT) for the first time. Different from the weak adsorption on CNTs, it is shown that glycine molecules tend to be chemisorbed to SiCNTs. There are three patterns for individual glycine molecule adsorbed on (8, 0) SiCNT, including monodentate, cycloaddition and dissociative ones, with the latter two patterns (E_{ads} ranges from −22.08 to −34.99 kcal/mol) more stable than monodentate ones (E_{ads} ranges from −8.16 to −21.14 kcal/mol). In addition, we also investigated the adsorption of multiple glycine molecules on various zigzag (n, 0) (n=7, 8, 9 and 10) SiCNTs. It is shown that totally n (n=7, 8, 9 and 10) molecules can be chemisorbed on one circle of the wall of the SiCNT at most. And the E_{ads} per glycine decreases gradually with increased tube diameter due to the curvature effects. For the adsorption of dehydrogenated glycine radicals, it is found that both the N-centered and C-centered ones can form stable complexes by attacking on (8, 0) SiCNT. Totally one monodentate and two bidentate adsorption configurations of N-centered radical and three monodentate configurations of C-centered one can be found. Note that the important half-metals can be obtained for the bidentate configurations from N-centered radical due to the hybridization state of radical and tube in one spin channel crossing the Fermi level, while the *p*-type semiconductor can be produced for the monodentate configurations from C-centered radical because the impurity state derived from the radical itself is closer to the edge of valence band above the Fermi level, which may be applied in building of electronic devices and metal-free catalysis. Finally, we found that the encapsulation of glycine molecule is exothermic and thus energetically favourable in the SiCNTs with the diameter larger than (9, 0) SiCNT. Present study is expected to be of promising applications in nano-device building and biotechnology.

1. Introduction

Because of their outstanding and unique mechanical, electronic, and optical properties, one-dimensional nanomaterials, as represented by carbon nanotubes (CNTs), have triggered tremendous interest to research fields in physics, chemistry, materials, electronics and engineering.[1–5] Their high electrical conductivity and strength have made them promising materials for new applications such as field emitters[6,7] and scanning probes.[8] In addition, a broad variety of bio-molecules, such as proteins, peptides, and nucleic acid bases are used to functionalize the CNTs, which are utilized in a wide range of bio-fields, such as molecular level electronics,[9,10] biochemical sensors,[11–14] drug delivery,[15] gene delivery,[16,17] as well as in therapeutic applications.[18]

However, numerous reports have shown that CNTs have toxicity which limits their promising bio-applications.[19–24] For example, CNTs were found to elicit pathological changes in the lungs, produce respiratory function impairments, damage the mitochondrial DNA in aorta, increase the percent of aortic plaque, and induce atherosclerotic lesions in the brachiocephalic artery of the heart.[25] In addition, another factor that hinders the use of CNTs in biological system is their poor solubility in physiological solutions. Compared with CNTs, the silicon carbide nanotubes (SiCNTs), which has been experimentally synthesized by the reaction of SiO with multiwalled CNTs, are of less toxic effect.[26,27] Furthermore, in contrast to the hydrophobicity of CNTs, the SiC surface is hydrophilic.[28,29] Theoretical calculations have already demonstrated that SiCNTs have intrinsically high reaction activity to many small molecules including CO,[30] HCN,[30] NO,[31] NNO,[31] NO_2,[32] CO_2,[33] O_2[34] and HCHO[35] due to its polar nature.

Amino acids are the elementary units for composing protein and can reflect the common chemical properties of complicated biomolecules.[36–38] Among the twenty available amino acids, glycine molecule (NH_2CH_2COOH) is the simplest one at reasonable computational cost, and the dehydrogenated glycine radicals have also been successfully produced in the gas-phase[39] reaction of positively charged phenyl radicals with the neutral glycine molecule as well as in liquid phase.[40] Understanding of

the interactions between nanotubes and amino acids are very important and may be helpful for the applications in biotechnology and nano-device. Therefore, we decide to perform a detailed theoretical study on the SiCNTs interaction with glycine molecules and radicals, such as the geometrical structures, energetics and electronic properties based on the density functional theory (DFT) for the first time.

2. Computational methods

The all-electron DFT calculations were carried out using the spin-polarized generalized-gradient approximation with the Perdew−Burke−Ernzerhof (PBE) functional[41] and the double numerical basis set including polarization function (DNP basis set) implemented in the Dmol^3 package.[42−44] Zigzag single-wall SiCNTs were chosen as the benchmark models. The periodic boundary condition was used with a tetragonal supercell of 35 Å × 35 Å × c Å, and c was taken to be triple of the one-dimensional lattice parameter of the target systems, which ensure that there is a lateral separation more than 16 Å between the centers. It is long enough that there is no direct interaction between neighbored amino acid molecules. For the current calculations, the convergence criteria between optimization cycles are chosen as 10^{-5} Ha for energy, 0.001 Ha·Å^{-1} for force field, 0.005 Å for displacement, and 4.8 Å for global orbital cutoff. The Brillouin zone was sampled by 1 × 1 × 5 special *k*-points using the Monkhorst−Pack scheme.[45] In addition, by using the linear/quadratic synchronous transit (LST/QST) method[46,47] we also searched for the transition states to explore the kinetic feasibility.

To evaluate the interaction between glycine molecule/radical and SiCNT, the adsorption energy (E_{ads}) was calculated according to the following equation (1):

$$E_{ads} = E_{(glycine-SiCNT)} - E_{glycine} - E_{SiCNT} \quad (1)$$

Where $E_{(glycine-SiCNT)}$ is the total energy of the complex consisting of glycine molecule/radical and SiCNT, while $E_{glycine}$ and E_{SiCNT} are the individual energies of glycine molecule/radical and SiCNT, respectively. Thus, the negative value of the E_{ads} indicates exothermic reaction. Due to the system we studied is very large, the necessary calculation of vibrational frequencies to obtain the ZPE is significantly computationally demanding. Although the Dmol^3 program can give approximate values extrapolated to T=0K in the output file, we found that it is of few impact on our results. Therefore, the ZPE contributions are not taken into account in our reported energies. The charge transfer (*Q*) between SiCNT and glycine was analyzed based on the Hirshfeld[48] method, which is independent on the basis set and used widely. For instance, the Hirshfeld charge was calculated in the analysis of CO_2 and HCHO molecules adsorbed on SiCNTs.[33,35] In order to predict the electronic properties, we also calculated the band structures and density of states (DOS) using denser 1 × 1 × 20 special *k*-points with the PBE functional. It should be noted that the correction for basis set superposition error (BSSE) was not considered within the calculation of the binding energy because Inada et al.[49] have proven that the numerical basis sets implemented in Dmol^3 can minimize or even eliminate BSSE.

It is known that, in spite of great improvement over LDA, a typical GGA type of DFT like the PBE method we used still underestimates the binding for the systems mainly arising from van der Waals interaction.[50] Thus, it is most likely that the present binding energies (refer to encapsulated systems) of glycine conformers (*trans*-I and *cis*-II) with SiCNTs are lower than real ones due to cumulative effects, while the other relatively strong chemical interactions including glycine molecules/radicals on the surface of SiCNTs should be proper.

In addition, it is worth noting that GGA/PBE generally results in a well-known and physically understood underestimation of the band gap. Various computational approaches can be used to correct the shortcomings of approximate DFT theories, including GW corrections[51] or some exact Hartree Fock (HF) exchange in the modern hybrid density functional (B3LYP, PBE0, HSE, etc.),[52-54] which can lead to substantially improved band gaps; however, they are significantly computationally demanding. Moreover, GGA/PBE predictions have proven useful for prediction of trends as shown by the numerous studies of the band gap of hydrogen passivated nanotubes,[55,56] fluorine-doped SiCNT,[57] and different small molecules adsorbed on SiCNTs.[34,35] Hence, we believe it is reasonable and quantitative to investigate the electronic properties of glycine adsorbed on SiCNTs using the GGA/PBE theory here.

3. Results and discussion

In section 3.1, the geometrical structures, energetics of glycine molecules interacting on the surface of SiCNTs will be discussed; in section 3.2, not only the geometrical structures and energetics but also the electronic properties of the adsorption of dehydrogenated glycine radicals will be investigated; in section 3.3, the encapsulation of glycine molecule into SiCNTs will be explored.

3.1 The Interaction of Glycine Molecule on the Surface of SiCNTs

For the calculations of glycine molecule, we just choose the two conformers of *trans*-I and *cis*-II in regard to the C−C bond in our calculations due to the large stabilities among its all possible confoermers[58-60] as shown in Fig. 1. The *trans*-I is energetically favorable than the *cis*-II by 4.36 kcal/mol at the PBEPBE/6-31G (d,p) level of theory implemented with Gaussian 09 package.[61] Note that the utilized exchange-correlation function of PBEPBE with the double-ζ polarized basis set 6-31G(d,p) in Gaussian 09[61] are equivalent to the PBE/DNP in Dmol^3.[62] In the following, we will consider the adsorption of the both conformers.

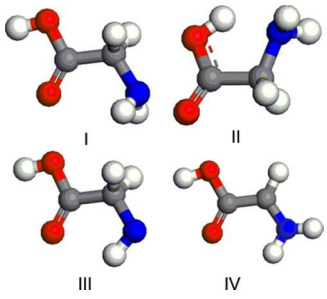

Fig. 1 The optimized structures of glycine molecules (*trans*-I and *cis*-II) and radicals (N-centered III and C-centered IV). Atom color code: blue for nitrogen; gray for carbon; red for oxygen; white for hydrogen.

3.1.1 Structures and Energetics of Individual Glycine Molecule Interacting with (8, 0) SiCNT

The stable adsorption geometry of a single glycine molecule on SiCNTs is studied at first. Taking (8, 0) SiCNT as example, the adsorption configurations of various functional groups of glycine molecule are optimized at the PBE/DNP level of theory, including $-NH_2$, =C=O and −OH in −COOH are close to the silicon atom (S site), carbon atom (C site), axial Si−C bond (BA site), zigzag Si−C bond (BZ site) or the hollow of six-membered ring (H site) in (8, 0) SiCNT, respectively, as sketched in Fig. 2a. After numerous attempts, it is found that there are three stable patterns of individual glycine molecule adsorption on the surface of SiCNT, including monodentate (Fig. 3a), cycloaddition (Fig. 3b), as well as dissociative adsorption (Fig. 3c).

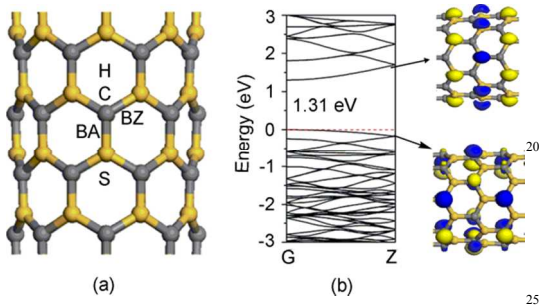

Fig. 2 (a) The structure models and various adsorption sites of (8, 0) SiCNT and (b) its band structures with their HOMOs and LUMOs at the Γ point with isosurface values of 0.03. C: carbon atom; S: silicon atom; BA: axial Si−C bond; BZ: zigzag Si−C bond; H: the hollow.

First, let's analyze the monodentate adsorption in detail. It is shown that three stable monodentate configurations (labeled as M_I-a, M_I-b and M_I-c) related to *trans*-I glycine molecule and three (M_{II}-a, M_{II}-b and M_{II}-c) related to *trans*-II one are obtained including the N atom in $-NH_2$, the O atom in =C=O and the O atom in −OH bonded to SiCNT as plotted in Fig. 3a, respectively. The calculated adsorption energy (E_{ads}), charge transfer (Q), and bond length (D) are summarized in Table 1. For all the six monodentate configurations (M_I-a, M_I-b, M_I-c and M_{II}-a, M_{II}-b, M_{II}-c), it is shown that the glycine molecules are tightly bonded to the Si atom of SiCNT. The corresponding bond lengths (D) of above six configurations are 2.03 ($D_{N\text{-}Si}$), 1.98 ($D_{O\text{-}Si}$), 1.96 ($D_{O\text{-}Si}$), 2.03 ($D_{N\text{-}Si}$), 1.93 ($D_{O\text{-}Si}$) and 2.03 Å ($D_{O\text{-}Si}$) with the corresponding E_{ads} at −21.14, −8.16, −9.46, −12.97, −15.02 and −8.21 kcal/mol, respectively, indicating that the interactions between glycine molecule and SiCNT are all exothermic and much stronger than that of pristine CNT (about 1.31 kcal/mol),[63] and the stable glycine/SiCNT complexes are formed. Besides, there is a remarkable charge transfer between the tubes and molecules with the maximum of Q at 0.18e (M_I-a), which is much larger than that of pristine CNT (about 0.01e).[63] This is understandable that the HOMOs of SiCNT are mainly centered on the 2p orbital of C atoms while LUMOs are located on the 3p orbital of Si atoms as shown in Fig. 2b, thus the electron-riched O and N atoms of the glycine molecule prefer to donate electrons to the LUMOs of the Si atoms, which increases the interaction between each other. At the same time, the Si atom adsorbed by glycine is pulled outward from the tube wall with the corresponding bond length of Si−C increased from 1.79 Å to 1.84 Å, resulting in the conversion from sp^2 to sp^3 hybridization.

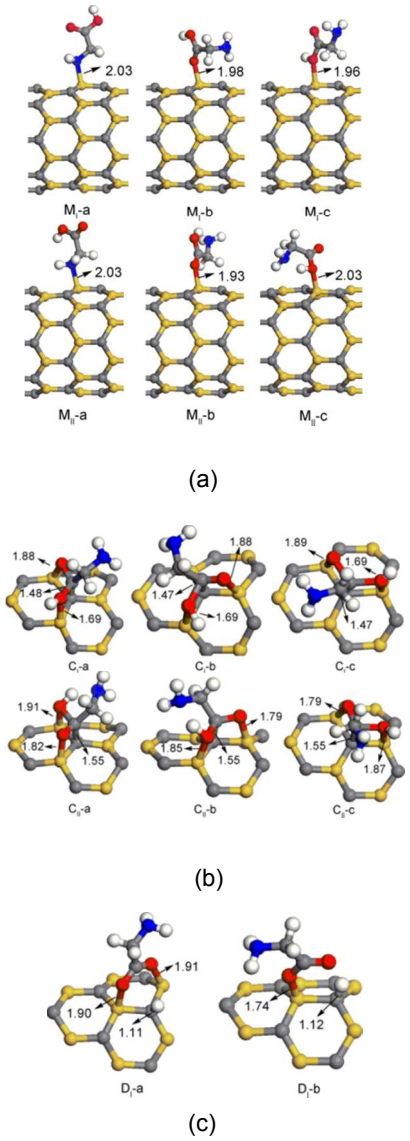

Fig. 3 The optimized of individual glycine molecule adsorbed on (8, 0) SiCNT with the (a) monodentate configurations for *trans*-I and *cis*-II; (b) cycloaddition configurations for *trans*-I and *cis*-II; (c) dissociation configurations for *trans*-I.

Second, we turn to study the cycloaddition adsorption labeled as C_I-a, C_I-b and C_I-c from *trans*-I conformer and C_{II}-a, C_{II}-b and C_{II}-c from *cis*-II one as shown in Fig. 3b. For all above six cycloaddition configurations, we found that the C=O bond in −COOH can connect with the Si−C bond at BA or BZ site parallelly, forming [2+2] four-membered rings. This is understandable that glycine molecule is a species with π-bond (C=O), which prefers to form cycloaddition with Si−C on nanotube. Similar adsorption patterns have been found on the π-type species of HCHO and HCOOH interacting with SiCNT[35,64] as well as O_2 and N_2 with AlNNT.[65] Note that the corresponding E_{ads} of the six cycloaddition configurations range from −22.08 to −34.99 kcal/mol as listed in Table 2, which are energetically more stable than monodentate ones.

At last, we will focus on the dissociative adsorption with

regard to H atom in −OH dissociation from glycine to SiCNT. As mentioned above, before initial optimization, we considered the dissociative adsorption of glycine not only at the Si atoms but also the C atoms and the other adsorption sites of SiCNT. However, after careful optimization, finally we can only find the dissociative adsorption at the Si atoms of SiCNT. Similar dissociative adsorption at the Si atoms can also be found in the HCOOH and H−OX (X=H, CH_3, and C_2H_5) dissociated on SiCNTs.[64,67] Two dissociative configurations of *trans*-I are obtained labeled as D_I-a and D_I-b as shown in Fig. 3c. In the more stable configuration of D_I-a, the two O atoms in −COOH are attached to the SiCNT, leading to the formation of two Si−O bonds (1.90 and 1.91Å) with E_{ads} at −34.58 kcal/mol and Q at 0.12e, respectively. Meanwhile, the H atom in −COOH is bonded to the surrounding C atom of SiCNT with the bond length of 1.11 Å, which is close to the typical C−H bond in methane,[66] indicating the strong covalent interaction between the H and nanotube. Moreover, the Si−C bond adsorbed by O and H atoms is elongated from 1.79 (pristine SiCNT) to 1.92 Å with the cleavage of O−H bond of −COOH. The similar cleavages of O−H bonds have been reported on the interaction of H−OX (X=H, CH_3, and C_2H_5) with SiCNT.[67] After numerous attempts of initial optimization configurations of cis-II glycine molecule on (8, 0) SiCNT, including various functional groups of cis-II glycine molecule (−NH_2, =C=O and −OH in −COOH) close to the silicon atom (S site), carbon atom (C site), axial Si−C bond (BA site), zigzag Si−C bond (BZ site) or the hollow of six-membered ring (H site) in (8, 0) SiCNT, however, we cannot find any dissociative adsorption configuration on the *cis*-II conformer. This may be rationalized that when the two O atoms in −COOH of *cis*-II are bonded to SiCNT, the orientation of H atom in −COOH is up deviated from SiCNT, and thus difficult to be absorbed by the SiCNT.

Taking the configuration C_I-a as example, we elucidate the process of glycine dissociated on SiCNT. As shown in Fig. 4, the weak physisorption configuration of the glycine molecule with SiCNT is considered as the initial state (IS) has been added the transition state (TS) and intermediate state (IM). When moving toward the SiCNT, the −COOH in glycine molecule is first broken down into formate and hydrogen forming Si−O and Si−H bonds with SiCNT barrierlessly to IM (−32.69kcal/mol). Starting from IM, the other O atom in formate group further forms another Si−O bond with the neighboring Si atom to form TS with a small barrier of 4.53 kcal/mol and then to product C_I-a. So, this dissociation process is both kinetically feasible and energetically favorable. Similar dissociative process can be found on HCOOH interacting with SiCNT.[64]

From the adsorption energy (E_{ads}), charge transfer (Q), and bond length (D) as listed in Table 1 and 2, all the three patterns of adsorption correspond to chemisorptions, which is in contrast to the physisorptions on CNT.[63] This indicates that the binding of glycine to SiCNT is stronger than that of CNT, leading to stable glycine/SiCNT complexes. For sensing or monitoring of protease activity, the stable glycine/SiCNT complexes should be essential in designing life sciences-related tools. However, all the above three patterns of adsorption remain the original semi-conductor with the band gap of 1.31 eV, just the same as that of pristine SiCNT as shown in Fig. S1 (see the Supporting Information 1), herein we do not discuss their electron properties further.

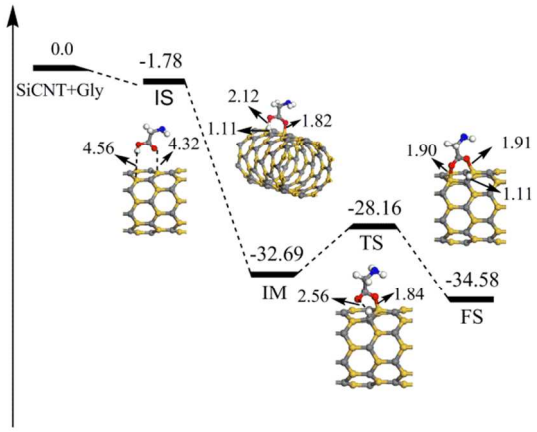

Fig. 4 Potential energy profiles for the dissociative adsorption of glycine on (8, 0) SiCNT based on configuration of C_I-a.

3.1.1 Multiple Glycine Molecules Interacting on the (8, 0) SiCNT

To better accord with the adsorption process in real environment, we need also to investigate the adsorption of multiple glycine molecules on SiCNT. Based on the most stable monodentate configuration of M_I-a with Si site for adsorption, when the second glycine molecule is added, two types of adsorption were considered, including the configurations at the opposite and adjacent sites related to the first glycine molecule as shown in Fig. 4a and 4b, respectively. It is shown that the more stable adsorption corresponds to two glycine molecules far from each other on the opposite sides of the tube (Fig. 5a) with the E_{ads} at −20.94 kcal/mol and Q at 0.18e per glycine molecule, which is approximately equal to that of the most stable configuration of M_I-a. The meta-stable adsorption corresponds to the configuration with two glycine molecules close to each other with the E_{ads} and Q at −18.63 kcal/mol and 0.17e, respectively, as shown in Fig. 5b. Note that the smaller steric repulsion between two opposite glycine molecules (Fig. 5a) should be responsible for its larger stability.

Based on above adsorption configurations with two molecules, more glycine molecules are adsorbed on the Si atoms in one circle of the wall of (8, 0) SiCNT. To minimize the steric repulsion, the added molecules are placed as far as possible from each other (Fig. 5c−h). It is clear that the adsorption eventually results in the formation of perfect ring structure of eight glycine molecules around the tube. The absolute value of E_{ads} and Q per molecule decreases gradually until to −11.23 kcal/mol and 0.13e due to their steric repulsion as shown in Fig. 6. Accordingly, the diameter of the tube is increased from 7.97 Å to 8.22 Å. Furthermore, we also calculated multiple glycine molecules adsorbed to (n, 0) (n=7, 9 and 10) SiCNTs based on configuration of M_I-a. It is shown that seven, nine and ten glycine molecules can be chemisorbed to the Si atoms of the tubes at most, that is, the maximum adsorption of (n, 0) SiCNT is n glycine molecules, as shown in Fig. S2. Table 3 summarizes the adsorption energy (E_{ads}) per glycine and bond length (D) for the adsorption on various zigzag SiCNTs. Because of the curvature effects, the E_{ads} decreases with the increase of the tube diameters. For example, the E_{ads} per glycine on the (7, 0) tube is −14.56 kcal/mol, while it decreases to −6.63 kcal/mol when adsorbed to the (10, 0) SiCNT

as listed in Table 3. Accordingly, the formed Si−N of SiCNT and glycine molecule increases gradually with the increase of the tube diameter, which further testify that the interaction becomes weaker due to curvature effects. Similar curvature effects were reported on the adsorption of multiple CO_2 and HCHO to SiCNTs.[33,35]

Note that, we consider multiple glycine molecules adsorbed on SiCNT based on the monodentate configuration of M_I-a just because: firstly, the configuration of M_I-a is energetically the most favorable among the monodentate configurations (Table 1). Secondly, although the cycloaddition configurations and dissociative configurations (Table 2) are more energetically favorable than the monodentate configuration of M_I-a, they may have larger steric repulsion between two neighboring glycine molecules. (Fig. 3). Note that the same model of multiple molecules adsorbed on nanotubes are uesed widely.[33,35,64]

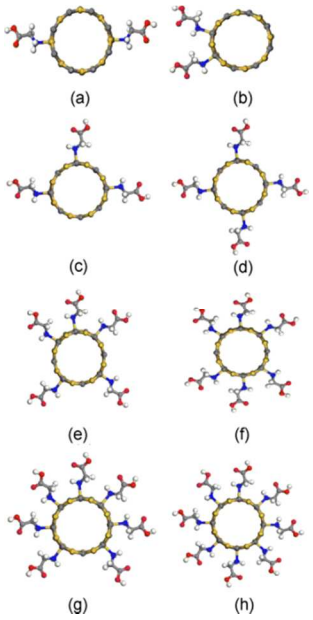

Fig. 5 The optimized configurations of multiple glycine molecules adsorbed on the (8, 0) SiCNT based on configuration of M_I-a.

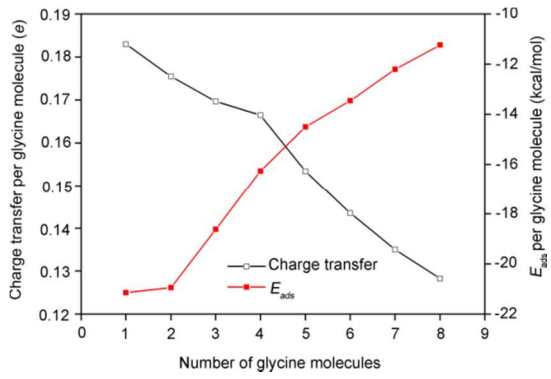

Fig. 6 The variation of adsorption energy and charge transfer (per glycine) as a function of the number of glycine molecules on (8, 0) SiCNT based on configuration of M_I-a.

3.2 The Interaction of Glycine Radicals on the Surface of SiCNT

Because the dehydrogenated radicals from *cis*-II glycine molecule is much less stable than the counterparts of *trans*-I,[39] we just considered the adsorption related to the dehydrogenated glycine radicals based on *trans*-I. Compare with previous works, among the possible isomers are the ones from which one hydrogen atom is abstracted either from the $-NH_2$ and the α-C[68], that is, the N-centered III and C-centered radicals IV, as shown in Fig. 1. Note that, similar to other commonly density functional theory (DFT) exchange-correlation (XC) functional, although the PBE we used in this work may also predict qualitatively different structures for glycine radicals due to possible delocalization and self-interaction errors,[69,70] we still consider this will not affect our main focus on the interaction of glycine radicals with SiCNTs rather than the configurations of the radicals themselves.

3.2.1 Structures and Energetics of Glycine Radicals Interacting with (8, 0) SiCNT

To predict the reactivity site of (8, 0) SiCNT with respect to the radical attack, the Fukui functions measuring the susceptibility of the charge density $\rho(r)$ with respect to the loss or gain of electrons were calculated via the equation (2)[71]. The Fukui functions (FFs) are determined using Fukui function Model as implemented in Dmol^3 program, which is based on the frontier orbital theory of Fukui and developed further by Parr and Yang.[72] The FFs are computed using the finite difference approximation which is a qualitative way of measuring and displaying the reactivity of regions of a molecule.

$$f(r) = \left(\frac{\partial \rho(r)}{\partial N}\right)_{v(r)} \quad (2)$$

From which, the nucleophilic $(f^+(r))$, electrophilic $(f^-(r))$, and radical attack $(f^0(r))$ can be evaluated, respectively. Herein, we just discuss the $(f^0(r))$, the larger value means the greater sensitivity to radical attack. As shown in Fig. 7a, the Si and C atoms in the (8, 0) SiCNT are likely to compete with each other when they interact with radicals. However, the electron acceptance ability of Si atom should be stronger than the C atom owing to 0.34e transferred from Si to C atom resulting in an electron hole of Si.[33]

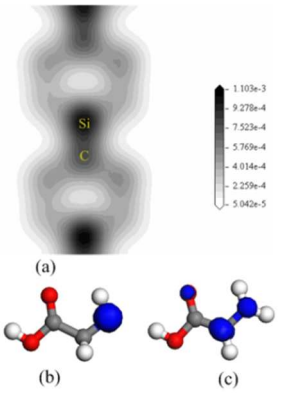

Fig. 7 (a) The contour of the Fukui functions of (8, 0) SiCNT. The highest and lowest values are indicated in the scale by the black and white colors, respectively; (b) The isodensity surfaces of the spin density of electron for the N-centered radical III with isosurface values of 0.2 a.u; (c) The isodensity surfaces of the spin density of electron for the C-centered radical IV with isosurface values of 0.2 a.u.

The isodensity surfaces of the spin density of electron for the N-centered III and C-centered radicals IV were also calculated as plotted in Fig. 7b and 7c, respectively. For the N-centered one III,

the N atom is located far from the O atoms, so the unpaired electron is almost "occupied" by the N atom itself only. As to the C-centered one, the α-C atom has lower electronegativity than that of neighbored N and O in =C=O. As a result, the unpaired electron is "shared" by the other two electronegative atoms to some extent, which is supported by the electronic distribution of spin density in Fig. 7c. So, we need only to consider the possible attack of the N atom of N-centered radical, as well as that of the O in =C=O, N and α-C atoms of C-centered radical.

After numerous optimizations, it is found that the N atom can interact with the (8, 0) SiCNT in three types for the attack of N-centered radical III, including one monodentate configuration of R_{III}-a and two bridged bidentate configurations of R_{III}-b and R_{III}-c, in which the N atom is right above Si or Si−C bonds with different bond orientations as shown in Fig. 8. For the monodentate configuration of R_{III}-a, the formed Si−N is 1.76 Å with the largest absolute value of E_{ads} (−51.81 kcal/mol) as shown in Table 4, indicating strong chemisorptions. For the two bidentate configurations of R_{III}-b and R_{III}-c, the C−N and Si−N bonds are formed between the N atom and tube at about 1.60 and 1.90 Å, respectively, giving rise to bridge adsorption configurations with lower E_{ads} at −23.93 and −15.17 kcal/mol. Accordingly, the Si−C bonds of SiCNT close to the adsorption sites are elongated to 1.88 and 1.94 Å, respectively. This is well consistent with previous reports about N and NH_x (x=1, 2, 3) groups interacting with semiconducting SiC nanotubes.[73]

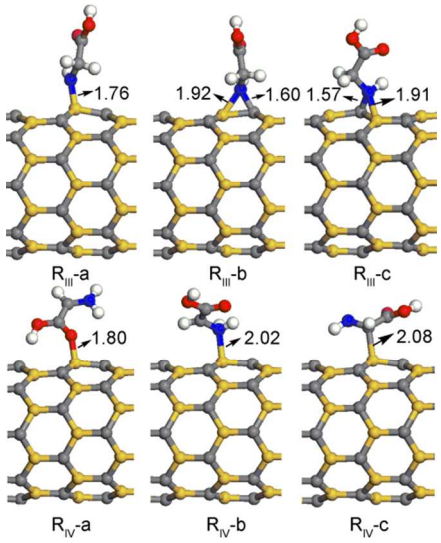

Fig. 8 The optimized configurations for glycine radicals absorbed on (8, 0) SiCNT for the N-centered radical III and the C-centered radical IV.

As for the attack of C-centered radical IV, three monodentate configurations with regard to different atoms interacting on the SiCNT are obtained as shown in Fig. 8. As discussed above, the Si atom of SiCNT is more sensitive to radical attack than C atom, thus the O, N or α-C atom that "share" the unpaired electron, tends to respectively interact with the Si atom in R_{IV}-a, R_{IV}-b and R_{IV}-c, as shown in Fig. 8. The corresponding bond lengths of Si−O, Si−N and Si−C are 1.80, 2.02 and 2.08Å with the E_{ads} at −22.34, −10.62 and −14.21 kcal/mol for R_{IV}-a, R_{IV}-b and R_{IV}-c, respectively.

From the formed covalent bonds and large E_{ads} as listed in Table 4, it is clear that both the N-centered and C-centered radicals interacting with SiCNT correspond to strong chemisorptions.

3.2.2 Electronic Properties of Glycine Radicals Interacting with (8, 0) SiCNT

Upon adsorption of glycine radicals, we found that the electronic properties of SiCNTs are significantly changed. For the adsorption of N-centered radical III, although the monodentate configuration of R_{III}-a has the largest E_{ads} (−51.81 kcal/mol), it is still a semiconductor with a band gap of 1.17 eV as shown in Fig. 9, which is just a minute change compared with the pristine (8, 0) SiCNT (Fig. 2b). This is not surprising since the strong binding between SiCNT and the N atoms just produces some stable structures with low-lying states in the band structure, which have minute impact on the band gap and valence states near the Fermi level, just similar to the phenomena reported on $-NH_3$ and N_2H_4 interacting with SiCNT.[74] However, the band structures of the bidentate configurations of R_{III}-b and R_{III}-c give rise to some new dispersive energy states near the Fermi level. From the plotted density of states (DOS) and frontier molecular orbital (FMO) as shown in Fig. 10 and S3, we can see that the new dispersive energy states are derived from the hybridization state of N-centered radical and tube. In the spin-up channels of configuration R_{III}-b and spin-down channel of R_{III}-c, it is found the Fermi levels cross the bottom of conduction band showing metallicity, while the other channels still have band gaps of 1.26 and 0.22 eV, respectively, indicating that half-metals are formed.

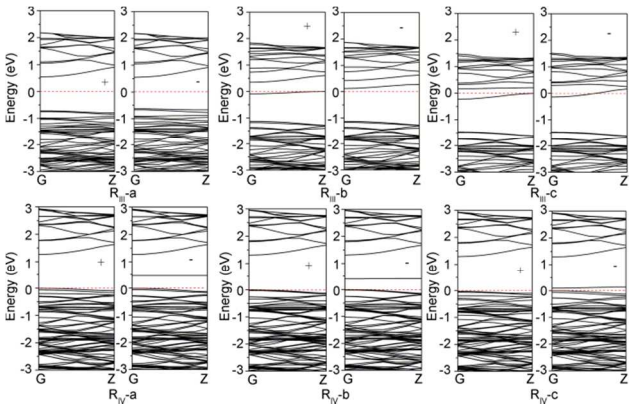

Fig. 9 The band structures of glycine radicals adsorbed on (8, 0) SiCNT. The spin-up and spin-down channels are distinguished with "+" and "–". The Fermi level is indicated with a red dotted line.

However, when the SiCNT is adsorbed with C-centered radical IV, the situation is different. It is found that a dispersive-free impurity state in the spin-down channel appears above on the Fermi level in the band structures of the three monodentate configurations (R_{IV}-a, R_{IV}-b and R_{IV}-c), while the spin-up channel is not modified as shown in Fig. 9. Taking the configuration of R_{IV}-a as example, it is found that in the spin-down channel there is a new impurity state emerged at 0.46 eV above the Fermi level, which is close and almost parallel to the edge of the valence band. This is mainly contributed from the local state of C-centered radical itself as indicated in DOS and FMO of Fig. 10 and S3, while the spin-up channel is not modified, which then dramatically reduces the band gap from 1.31 to 0.46 eV, resulting in a *p*-type semi-conductor. For the rest configurations of R_{IV}-b

and R_{IV}-c, through analysis of the band structures and DOS as shown in Fig. 9 and 10, respectively, it is also found that they both present *p*-type semi-conductors.

Therefore, the adsorptions with the bidentate configurations of N-centered radical on SiCNT can produce half-metals, which is very important in view of their possible application in spintronics with the electron transport through only one spin channel. While the monodentate adsorption configurations of C-centered radical can produce *p*-type semi-conductors, which may be applied in building of semi-conductor device, such as transistor, p-n junction photosensor and so on.

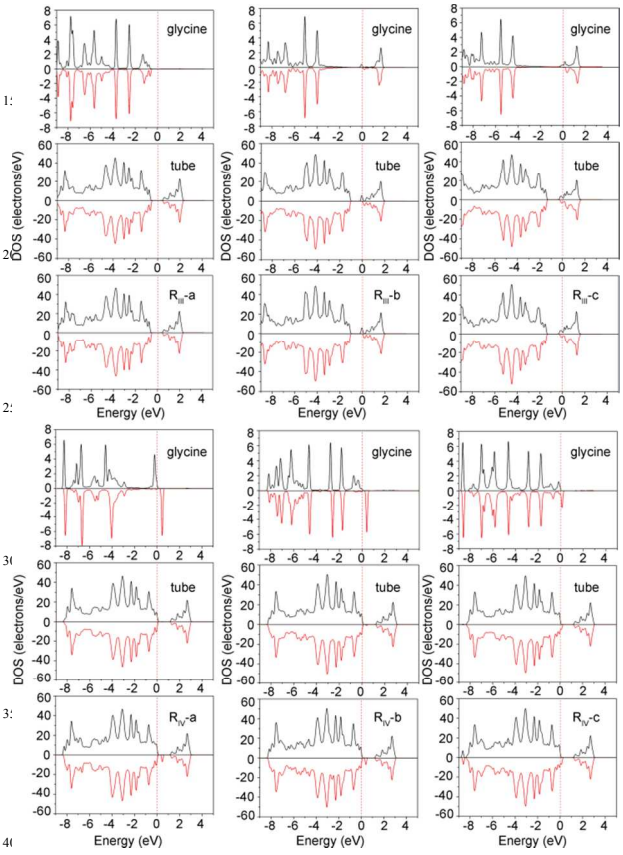

Fig. 10 The density of states (DOS) of glycine radicals adsorbed on (8, 0) SiCNT. The labels "glycine" and "tube" denote the projected DOS (PDOS) of the molecule and tube in the adsorbed system, respectively. The spin-up and spin-down channels in the DOS are plotted with black and red lines, respectively. The Fermi level is set to zero.

3.3 Encapsulation of Glycine Molecule within the SiCNTs

Due to the capacious interior of the SiCNT, it may be used as container to reserve glycine molecule. When one glycine molecule encapsulated into the (8, 0) SiCNT, both the tube and molecules deform slimly as shown in Fig. 11. However, from the binding energies of 6.13 and 1.15 kcal/mol for the encapsulation of *trans*-I and *cis*-II molecule as shown in Fig. 12, both correspond to endothermic processes. In the case of smaller (7, 0) SiCNT, the binding energies are even positive at 45.31 and 40.11 kcal/mol, indicating energetically more unstable encapsulations.

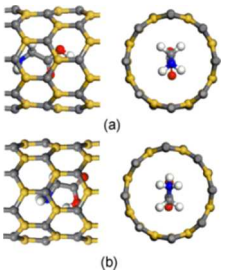

Fig. 11 The optimized structures of (a) *trans*-I and (b) *cis*-II glycine molecules encapsulated in (8, 0) SiCNT.

However, for the encapsulations in larger (9, 0) SiCNT, it is shown that the binding energies are negative at −3.62 and −8.34 kcal/mol, respectively, indicating exothermal processes. For the larger (10, 0) SiCNT, the binding energies of the *trans*-I and *cis*-II molecule are more negative at −22.74 and −28.12 kcal/mol, respectively. At the same time, there are no deformations found for both the tube and molecules. This implies that the encapsulations in (9, 0) and (10, 0) SiCNTs are energetically favourable. The present result indicates the zigzag SiCNTs with the diameter larger than (9, 0) can be potential containers to reserve glycine molecules, which can be applied for glycine storage and delivery.

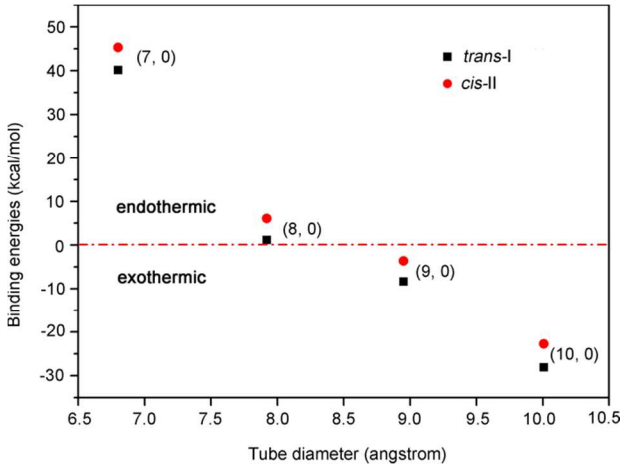

Fig. 12 The plotted binding energies per glycine molecule in the encapsulation process for the (n, 0) (n=7, 8, 9 and 10) SiCNTs, respectively.

4. Conclusions

In summary, we have performed a detailed theoretical study on the geometrical structures, energetics and electronic properties on SiCNTs interacting with glycine molecules and radicals based on density functional theory (DFT) for the first time. Unlike the weak interaction of glycine molecule on CNT, it is shown that individual glycine molecule tends to be chemisorbed to the (8, 0) SiCNT with three patterns, that is, monodentate, cycloaddition and dissociative adsorption, with the latter two adsorption patterns (E_{ads} ranges from −22.08 to −34.99 kcal/mol) more stable than monodentate ones (E_{ads} ranges from −8.16 to −21.14 kcal/mol). In addition, we also studied multiple glycine molecules adsorption on various zigzag (n, 0) (n=7, 8, 9 and 10) SiCNTs. It is shown that n glycine molecules can be chemisorbed on one circle of the wall of the SiCNTs at most, and the E_{ads} per glycine

decreases gradually with increased tube diameter because of the curvature effects. For the adsorption of dehydrogenated glycine radicals, both the N-centered and C-centered ones can also be chemisorbed to form quite stable complexes with (8, 0) SiCNTs. Totally one monodentate and two bidentate configurations corresponding to N-centered radical and three monodentate configurations of C-centered radical can be found. It should be noted that the adsorption with bidentate configurations of N-centered radical will result in half-metals due to the hybridization state of radical and tube, which crosses the Fermi level in one spin channel, while that monodentate configurations of C-centered one will produce *p*-type semi-conductors because the impurity state derived from the radical itself is close to the edge of valence band above the Fermi level, implying their promising application in building electronic devices and metal-free catalysis. The encapsulation of glycine molecule is endothermic for the (7, 0) and (8, 0) SiCNTs in contrast to the exothermicity for the (9, 0) and (10, 0) SiCNTs, implying that zigzag SiCNTs with the diameter larger than (9, 0) can be potential containers to reserve glycine molecules. Present study is hoped to be of promising applications in nano-device building and biotechnology and stimulating the experimental research in future.

Acknowledgements

This work is supported by National Natural Science Foundation of China (No. 21173095), Guangdong Natural Science Foundation (No. S2013010014476) and Engagement Fund of Shantou University (No. NFC13001).

Notes and references

[a] *Department of Chemistry, Shantou University, Guangdong, 515063, P. R. China. Tel: +86 (754) 8650 2917; E-mail: ghchen@stu.edu.cn*
[b] *State Key Laboratory of Theoretical and Computational Chemistry, Institute of Theoretical Chemistry, Jilin University, Changchun, 130023, P. R. China.*

1 S. Iijima, *nature*, 1991, **354**, 56-58.
2 S. Iijima and T. Ichihashi, 1993.
3 R. Antonov and A. Johnson, *Physical review letters*, 1999, **83**, 3274.
4 P. Avouris, *Accounts of Chemical Research*, 2002, **35**, 1026-1034.
5 S. Tatsuura, M. Furuki, Y. Sato, I. Iwasa, M. Tian and H. Mitsu, *Advanced Materials*, 2003, **15**, 534-537.
6 W. A. De Heer, A. Chatelain and D. Ugarte, *Science*, 1995, **270**, 1179-1180.
7 N. De Jonge, Y. Lamy, K. Schoots and T. H. Oosterkamp, *Nature*, 2002, **420**, 393-395.
8 P. Hansma, J. Cleveland, M. Radmacher, D. Walters, P. Hillner, M. Bezanilla, M. Fritz, D. Vie, H. Hansma and C. Prater, *Applied Physics Letters*, 1994, **64**, 1738-1740.
9 K. Bradley, M. Briman, A. Star and G. Grüner, *Nano Letters*, 2004, **4**, 253-256.
10 Z. Kuang, S. N. Kim, W. J. Crookes-Goodson, B. L. Farmer and R. R. Naik, *Acs Nano*, 2009, **4**, 452-458.
11 R. Azamian, J. J. Davis, K. S. Coleman, C. B. Bagshaw and M. L. Geen, *Journal of the American Chemical Society*, 2002, **124**, 12664-12665.
12 D. Vardanega, F. Picaud and C. Girardet, *The Journal of chemical physics*, 2007, **127**, 194702.
13 M. F. Mora, C. E. Giacomelli and C. D. Garcia, *Analytical chemistry*, 2009, **81**, 1016-1022.
14 G. Abadir, K. Walus and D. Pulfrey, *Nanotechnology*, 2010, **21**, 015202.
15 J. T. Robinson, K. Welsher, S. M. Tabakman, S. P. Sherlock, H. Wang, R. Luong and H. Dai, *Nano research*, 2010, **3**, 779-793.
16 Q. Lu, J. M. Moore, G. Huang, A. S. Mount, A. M. Rao, L. L. Larcom and P. C. Ke, *Nano Letters*, 2004, **4**, 2473-2477.
17 J. McCarroll, H. Baigude, C.-S. Yang and T. M. Rana, *Bioconjugate chemistry*, 2009, **21**, 56-63.
18 H. J. Lee, J. Park, O. J. Yoon, H. W. Kim, W. B. Lee, N.-E. Lee, J. V. Bonventre and S. S. Kim, *Nature Nanotechnology*, 2011, **6**, 121-125.
19 H. J. Johnston, G. R. Hutchison, F. M. Christensen, S. Peters, S. Hankin, K. Aschberger and V. Stone, *Nanotoxicology*, 2010, **4**, 207-246.
20 C.-w. Lam, J. T. James, R. McCluskey, S. Arepalli and R. L. Hunter, *CRC Critical Reviews in Toxicology*, 2006, **36**, 189-217.
21 L. Murr, K. Garza, K. Soto, A. Carrasco, T. Powell, D. Ramirez, P. Guerrero, D. Lopez and J. r. Venzor, *International journal of environmental research and public health*, 2005, **2**, 31-42.
22 N. W. Shi Kam, T. C. Jessop, P. A. Wender and H. Dai, *Journal of the American Chemical Society*, 2004, **126**, 6850-6851.
23 M. Bottini, S. Bruckner, K. Nika, N. Bottini, S. Bellucci, A. Magrini, A. Bergamaschi and T. Mustelin, *Toxicology letters*, 2006, **160**, 121-126.
24 C. Ge, J. Du, L. Zhao, L. Wang, Y. Liu, D. Li, Y. Yang, R. Zhou, Y. Zhao and Z. Chai, *Proceedings of the National Academy of Sciences*, 2011, **108**, 16968-16973.
25 E.-J. Park, J. Roh, S. N. Kim, M.-S. Kang, B.-S. Lee, Y. Kim and S. Choi, *PloS one*, 2011, **6**, e25892.
26 J. N. Mwangi, N. Wang, A. Ritts, J. L. Kunz, C. G. Ingersoll, H. Li and B. Deng, *Environmental Toxicology and Chemistry*, 2011, **30**, 981-987.
27 R. Moradian, S. Behzad and R. Chegel, *Physica B: Condensed Matter*, 2008, **403**, 3623-3626.
28 G. Cicero, G. Galli and A. Catellani, *The Journal of Physical Chemistry B*, 2004, **108**, 16518-16524.
29 H. H. Haeri, S. Ketabi and S. M. Hashemianzadeh, *Journal of molecular modeling*, 2012, **18**, 3379-3388.
30 R. Wu, M. Yang, Y. Lu, Y. Feng, Z. Huang and Q. Wu, *The Journal of Physical Chemistry C*, 2008, **112**, 15985-15988.
31 G. Gao and H. S. Kang, *Journal of Chemical Theory and Computation*, 2008, **4**, 1690-1697.
32 G. Gao, S. H. Park and H. S. Kang, *Chemical Physics*, 2009, **355**, 50-54.
33 J.-x. Zhao and Y.-h. Ding, *Journal of Chemical Theory and Computation*, 2009, **5**, 1099-1105.
34 F. Cao, X. Xu, W. Ren and C. Zhao, *The Journal of Physical Chemistry C*, 2009, **114**, 970-976.
35 X. Wang and K. Liew, *The Journal of Physical Chemistry C*, 2011, **115**, 10388-10393.
36 V. Zorbas, A. L. Smith, H. Xie, A. Ortiz-Acevedo, A. B. Dalton, G. R. Dieckmann, R. K. Draper, R. H. Baughman and I. H. Musselman, *Journal of the American Chemical Society*, 2005, **127**, 12323-12328.
37 W. Fan, J. Zeng and R. Zhang, *Journal of Chemical Theory and Computation*, 2009, **5**, 2879-2885.
38 Y. Wang and H. Ai, *The Journal of Physical Chemistry B*, 2009, **113**, 9620-9627.
39 Y. Huang, L. Guler, J. Heidbrink and H. Kenttämaa, *Journal of the American Chemical Society*, 2005, **127**, 3973-3978.
40 M. Bonifac˘ic, I. Štefanic, G. L. Hug, D. A. Armstrong and K.-D. Asmus, *Journal of the American Chemical Society*, 1998, **120**, 9930-9940.
41 J. P. Perdew, K. Burke and M. Ernzerhof, *Physical review letters*, 1996, **77**, 3865.
42 B. Delley, *The Journal of chemical physics*, 1990, **92**, 508-517.
43 B. Delley, *The Journal of chemical physics*, 1991, **94**, 7245.
44 B. Delley, *International journal of quantum chemistry*, 1998, **69**, 423-433.
45 H. J. Monkhorst and J. D. Pack, *Physical Review B*, 1976, **13**, 5188-5192.
46 G. Henkelman and H. Jonsson, *The Journal of chemical physics*, 2000, **113**, 9978-9985.
47 R. Olsen, G. Kroes, G. Henkelman, A. Arnaldsson and H. Jónsson, *The Journal of chemical physics*, 2004, **121**, 9776-9792.
48 F. Hirshfeld, *Theoretica chimica acta*, 1977, **44**, 129-138.

49Y. Inada and H. Orita, *Journal of computational chemistry*, 2008, **29**, 225-232.

50 M. Delle Piane, M. Corno and P. Ugliengo, *Journal of Chemical Theory and Computation*, 2013, **9**, 2404-2415.

51 W. G. Aulbur, L. Jönsson and J. W. Wilkins, *Solid State Physics*, 1999, **54**, 1-218.

52 J. K. Perry, J. Tahir-Kheli and W. A. Goddard III, *Physical Review B*, 2001, **63**, 144510.

43 C. Adamo and V. Barone, *The Journal of chemical physics*, 1999, **110**, 6158-6170.

54 J. Heyd, J. E. Peralta, G. E. Scuseria and R. L. Martin, *The Journal of chemical physics*, 2005, **123**, 174101.

55 O. Hod and G. E. Scuseria, *ACS nano*, 2008, **2**, 2243-2249.

56 V. Barone, J. Heyd and G. E. Scuseria, *The Journal of chemical physics*, 2004, **120**, 7169-7173.

57 X. Wang and K. M. Liew, *The Journal of Physical Chemistry C*, 2012, **116**, 1702-1708.

58 V. Barone, C. Adamo and F. Lelj, *The Journal of chemical physics*, 1995, **102**, 364-370.

59 V. Barone, M. Biczysko, J. Bloino and C. Puzzarini, *Physical Chemistry Chemical Physics*, 2013, **15**, 1358-1363.

60 A. G. Csaszar, *Journal of the American Chemical Society*, 1992, **114**, 9568-9575.

61 M. Frisch, G. Trucks, H. B. Schlegel, G. Scuseria, M. Robb, J. Cheeseman, G. Scalmani, V. Barone, B. Mennucci and G. Petersson, *Inc., Wallingford, CT*, 2009, **270**, 271.

62 P. C. Hariharan and J. A. Pople, *Theoretica chimica acta*, 1973, **28**, 213-222.

63 W. Sun, Y. Bu and Y. Wang, *The Journal of Physical Chemistry B*, 2008, **112**, 15442-15449.

64 Y. Chen, H.-x. Wang, J.-x. Zhao, X.-g. Wang, Q.-h. Cai, Y.-h. Ding and X.-z. Wang, *Journal of Nanoparticle Research*, 2012, **14**, 1-11.

65 W.-g. Liu, G.-h. Chen, X.-c. Huang, D. Wu and Y.-p. Yu, *The Journal of Physical Chemistry C*, 2012, **116**, 4957-4964.

66 M. Zhao, Y. Xia, R. Zhang and S.-T. Lee, *The Journal of chemical physics*, 2005, **122**, 214707.

67 J.-x. Zhao, B. Xiao and Y.-h. Ding, *The Journal of Physical Chemistry C*, 2009, **113**, 16736-16740.

68 D. Yu, A. Rauk and D. A. Armstrong, *Journal of the American Chemical Society*, 1995, **117**, 1789-1796.

69 V. B. Oyeyemi, J. A. Keith, M. Pavone and E. A. Carter, *The Journal of Physical Chemistry Letters*, 2012, **3**, 289-293.

70 E. I. Izgorodina, D. R. Brittain, J. L. Hodgson, E. H. Krenske, C. Y. Lin, M. Namazian and M. L. Coote, *The Journal of Physical Chemistry A*, 2007, **111**, 10754-10768.

71 R. G. Parr and W. Yang, *Journal of the American Chemical Society*, 1984, **106**, 4049-4050.

72 R. G. Parr and W. Yang, Density-functional theory of atoms and molecules, *Oxford university press*, 1989.

73 T. He, M. Zhao, Y. Xia, W. Li, C. Song, X. Lin, X. Liu and L. Mei, *The Journal of chemical physics*, 2006, **125**, 194710.

74 X. Zhou and W. Q. Tian, *The Journal of Physical Chemistry C*, 2011, **115**, 11493-11499.

Cite this: DOI: 10.1039/c0xx00000x

www.rsc.org/xxxxxx

ARTICLE TYPE

Figure Captions

Fig. 1 The optimized structures of glycine molecules (*trans*-I and *cis*-II) and radicals (N-centered III and C-centered IV). Atom color code: blue for nitrogen; gray for carbon; red for oxygen; white for hydrogen.

Fig. 2 (a) The structure models and various adsorption sites of (8, 0) SiCNT and (b) its band structures with their HOMOs and LUMOs at the Γ point with isosurface values of 0.03. C: carbon atom; S: silicon atom; BA: axial Si−C bond; BZ: zigzag Si−C bond; H: the hollow.

Fig. 3 The optimized of individual glycine molecule adsorbed on (8, 0) SiCNT with the (a) monodentate configurations for *trans*-I and *cis*-II; (b) cycloaddition configurations for *trans*-I and *cis*-II; (c) dissociation configurations for *trans*-I.

Fig. 4 Potential energy profiles for the dissociative adsorption of glycine on (8, 0) SiCNT based on the configuration of C_I-a.

Fig. 5 The optimized configurations of multiple glycine molecules adsorbed on the (8, 0) SiCNT based on configuration of M_I-a.

Fig. 6 The variation of adsorption energy and charge transfer (per glycine) as a function of the number of glycine molecules on (8, 0) SiCNT based on configuration of M_I-a.

Fig. 7 (a) The contour of the Fukui functions of (8, 0) SiCNT. The highest and lowest values are indicated in the scale by the black and white colors, respectively; (b) The isodensity surfaces of the spin density of electron for the N-centered radical III with isosurface values of 0.2 a.u; (c) The isodensity surfaces of the spin density of electron for the C-centered radical IV with isosurface values of 0.2 a.u.

Fig. 8 The optimized configurations for glycine radicals absorbed on (8, 0) SiCNT for the N-centered radical III and the C-centered radical IV.

Fig. 9 The band structures of glycine radicals adsorbed on (8, 0) SiCNT. The spin-up and spin-down channels are distinguished with "+" and "−". The Fermi level is indicated with a red dotted line.

Fig. 10 The density of states (DOS) of glycine radicals adsorbed on (8, 0) SiCNT. The labels "glycine" and "tube" denote the projected DOS (PDOS) of the molecule and tube in the adsorbed system, respectively. The spin-up and spin-down channels in the DOS are plotted with black and red lines, respectively. The Fermi level is set to zero.

Fig. 11 The optimized structures of (a) *trans*-I and (b) *cis*-II glycine molecules encapsulated in (8, 0) SiCNT.

Fig. 12 The plotted binding energies per glycine molecule in the encapsulation process for the (n, 0) (n=7, 8, 9 and 10) SiCNTs, respectively.

Supporting Information

Figure S1. The band structures of individual glycine molecule adsorbed on (8, 0) SiCNT with the (a) monodentate configurations for *trans*-I and *cis*-II; (b) cycloaddition configurations for *trans*-I and *cis*-II as well as dissociation configurations for *trans*-I. The Fermi level is dotted with a red line.

Figure S2. The optimized configurations of maximum number of glycine molecules adsorbed on the (n, 0) (n=7, 8, 9 and10) SiCNTs based on the configuration of M_I-a.

Figure S3. The plotted HOMO and LUMO of glycine radicals adsorbed on (8, 0) SiCNT with isosurface values of 0.03 a.u.

Cite this: DOI: 10.1039/c0xx00000x

www.rsc.org/xxxxxx

ARTICLE TYPE

TABLE 1: Calculated Bond Lengths (D), Band Gaps, Adsorption Energies (E_{ads}) and Charge Transfer (Q) of Monodentate Configurations for Individual Glycine Molecule (*trans*-I and *cis*-II) Adsorbed on the Surface of (8, 0) SiCNT. All of the Configurations and Corresponding Distances Are Given in Figure 3a.

	Configuration	D (Å)	Gap[c] (eV)	E_{ads} (kcal/mol)	Q[d] (| e |)
***trans*-I**	M_I-a	2.03 (D_{Si-N})	1.31	−21.14	0.18
	M_I-b	1.98 (D_{Si-O}[a])	1.31	−8.16	0.14
	M_I-c	1.96 (D_{Si-O}[b])	1.31	−9.46	0.13
***cis*-II**	M_{II}-a	2.03 (D_{Si-N})	1.31	−12.97	0.15
	M_{II}-b	1.93 (D_{Si-O}[a])	1.31	−15.02	0.16
	M_{II}-c	2.03 (D_{Si-O}[b])	1.31	−8.21	0.12

[a] The O[a] refers to O atom of =C=O and O[b] refers to O atom of −OH in glycine. [c]The HOMO−LUMO energy gap was calculated using the Γ point. [d]The amount of charges transfer from glycine molecules to (8, 0) SiCNT.

TABLE 2: Calculated Bond Lengths (D), Band Gaps, Adsorption Energies (E_{ads}) and Charge Transfer (Q) of Cycloaddition Configurations for Individual Glycine Molecule (*trans*-I and *cis*-II) and Dissociative Configurations for Individual Glycine Molecule (*trans*-I) Adsorbed on (8, 0) SiCNT. All of the Configurations and Corresponding Distances Are Given in Figure 3b and 3c.

	Configuration	D (Å)	Gap[c] (eV)	E_{ads} (kcal/mol)	Q[d] (| e |)
***trans*-I**	C_I-a	1.48(D_{C-C}) 1.88(D_{Si-O}[a]) 1.69(D_{Si-O}[b])	1.31	−28.85	0.21
	C_I-b	1.47(D_{C-C}) 1.88(D_{Si-O}[a]) 1.69(D_{Si-O}[b])	1.31	−34.99	0.17
	C_I-c	1.47(D_{C-C}) 1.89(D_{Si-O}[a]) 1.69(D_{Si-O}[b])	1.31	−31.09	0.18
***cis*-II**	C_{II}-a	1.55(D_{C-C}) 1.91(D_{Si-O}[a]) 1.82(D_{Si-O}[b])	1.31	−26.66	0.20
	C_{II}-b	1.55(D_{C-C}) 1.85(D_{Si-O}[a]) 1.79(D_{Si-O}[b])	1.31	−22.08	0.17
	C_{II}-c	1.55(D_{C-C}) 1.87(D_{Si-O}[a]) 1.79(D_{Si-O}[b])	1.31	−24.27	0.18
***trans*-I**	D_I-a	1.91(D_{Si-O}[a]) 1.90(D_{Si-O}[b]) 1.11(D_{C-H})	1.31	−34.58	0.12
	D_I-b	1.74(D_{Si-O}[a]) 1.12(D_{C-H})	1.31	−32.94	0.13

[a]The O[a] refers to O atom of =C=O and O[b] refers to O atom of −OH in glycine. [c]The HOMO−LUMO energy gap was calculated using the Γ point. [d]The amount of charge transfer from glycine molecules to (8, 0) SiCNT.

TABLE 3: Calculated Adsorption Energies (E_{ads}) per Molecule of Multiple Glycine Molecules Adsorbed on Various Zigzag (n, 0) SiCNTs Based on Configuration of M_1-a. All of the Corresponding Configurations and Corresponding Distances Are Given in Figure S2.

SiCNT	Diameter (Å)	Adsorption Number	E_{ads} (kcal/mol)	D_{Si-N} (Å)
(7, 0)	7.01	7	−14.56	1.98
(8, 0)	7.97	8	−11.23	2.05
(9, 0)	8.95	9	−9.37	2.09
(10, 0)	10.01	10	−6.63	2.12

TABLE 4: Calculated Bond Lengths (D), Band Gaps and Adsorption Energies (E_{ads}) of Glycine Radicals (N-centered III and C-centered IV) Adsorbed on the Surface of (8, 0) SiCNT. All of the Configurations and the Corresponding Distances Are Given in Figure 7.

	Configuration	D (Å)	Gap[a] (eV)	E_{ads} (kcal/mol)
N-centered III	R_{III}-a	1.76 ($D_{Si–N}$)	1.17	−51.81
	R_{III}-b	1.60 ($D_{Si–N}$) 1.92 ($D_{C–N}$)	-	−23.93
	R_{III}-c	1.57 ($D_{Si–N}$) 1.91 ($D_{C–N}$)	-	−15.17
C-centered IV	R_{IV}-a	1.80 ($D_{Si–O}$)	0.46	−22.34
	R_{IV}-b	2.02 ($D_{Si–N}$)	0.44	−22.34
	R_{IV}-c	2.08 ($D_{Si–C}$)	0.11	−14.21

[a]The HOMO−LUMO energy gap was calculated using the Γ point.

Cite this: DOI: 10.1039/c0xx00000x

www.rsc.org/xxxxxx

ARTICLE TYPE

Supporting information

Figure S1(a).

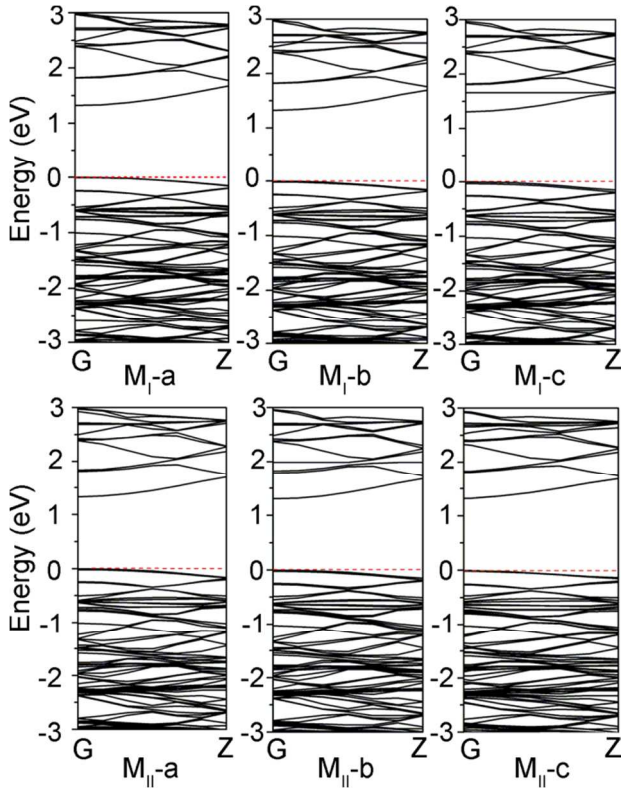

Figure S1(b).

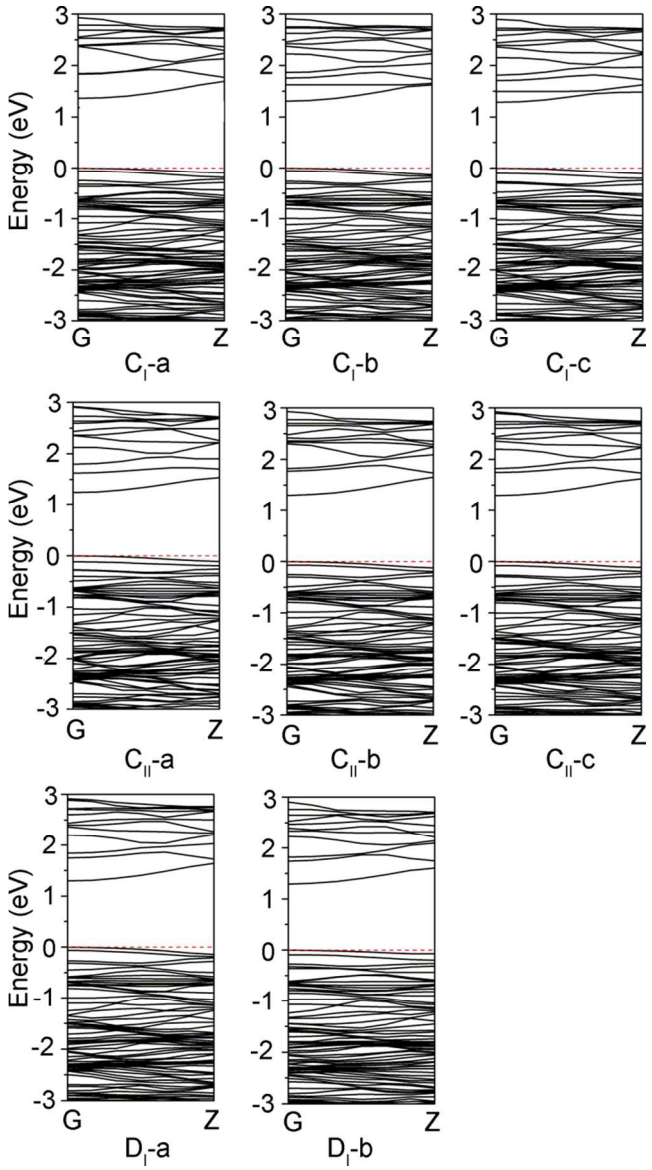

Figure S2.

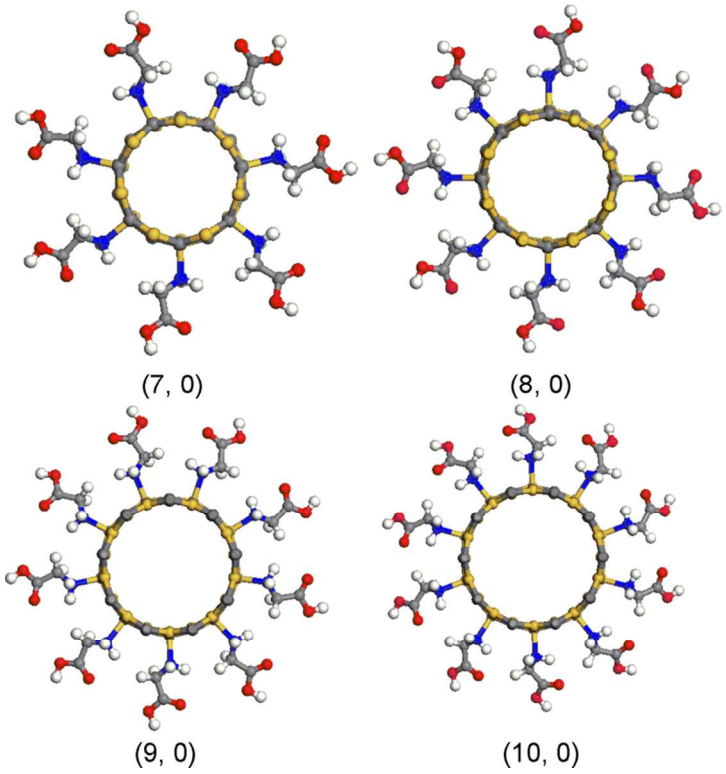

Figure S3.

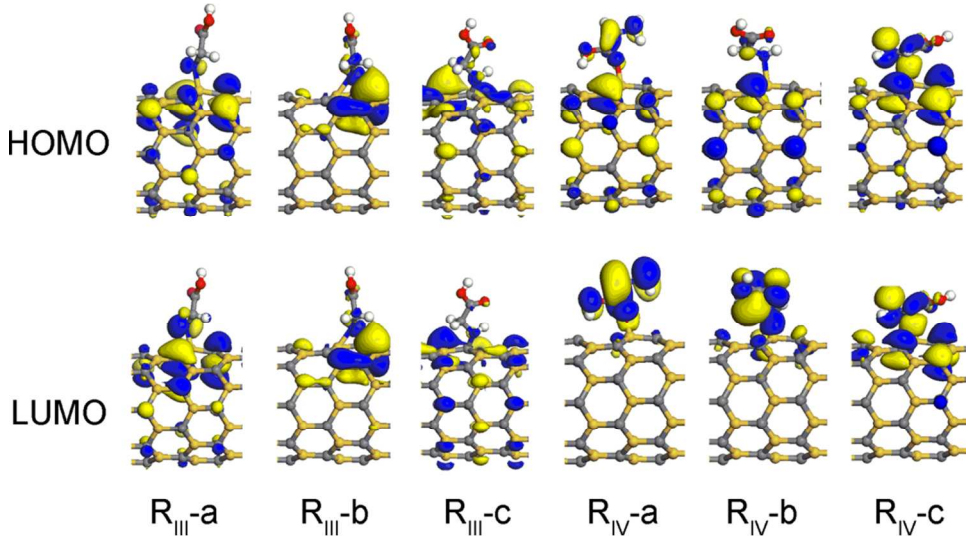

Table of Contents (TOC) Image